

# Mixed boundary conditions in $\text{AdS}_2/\text{CFT}_1$ from the coupling with a Kalb-Ramond field

Diego H. Correa, Maximiliano G. Ferro and Victor I. Giraldo-Rivera

*Instituto de Física La Plata - CONICET &  
Departamento de Física, Universidad Nacional de La Plata  
C.C. 67, 1900, La Plata, Argentina*

September 23, 2024

## Abstract

The open string dual to a  $1/6$  BPS Wilson line in the  $\mathcal{N} = 6$  super Chern-Simons-matter theory is coupled to a flat Kalb-Ramond field. We show that the resulting boundary term imposes mixed boundary conditions on the fields that describe the fluctuations on the world-sheet. These boundary conditions fix a combination of the derivatives of the fluctuations, parallel and transverse to the boundary. We holographically compute the correlation functions of insertions on the Wilson line in terms of world-sheet Witten diagrams. We observe that their functional dependence is consistent with the conformal symmetry on the line.

## 1 Introduction

The dynamics of fields propagating within Anti-de Sitter (AdS) space is known to encode the set of correlation functions of certain conformal field theories (CFTs) [1–3]. The presence of a boundary in AdS implies that different boundary conditions for fields give rise to diverse behaviors and properties in the corresponding dual CFT. For massive scalar fields, there exists a range of masses for which two different scaling dimensions are admissible for the dual primary operators, associated with either imposing the so-called *regular* or *alternate* boundary conditions [4]. Additionally, within the same mass range, it is also possible to impose certain mixed boundary conditions that are related to field theory operators interpolating between primaries of different scaling dimensions. These mixed boundary conditions are interpreted in terms of flows of the renormalization group [5–8].

For massless scalar fields in  $\text{AdS}_2$ , a different type of boundary conditions that mix longitudinal and transverse derivatives was considered in [9]. Since the mixing parameter is dimensionless in that case, one might expect these boundary conditions to be associated with a marginal deformation rather than with a flow of the renormalization group. However, determining whether these boundary conditions correspond to a conformal theory on the line or not, is not straightforward, as this will depend on the actual details of the  $\text{AdS}_2/\text{CFT}_1$  realization.

Massless scalar fields in  $\text{AdS}_2$  typically arise when studying the fluctuations on an open string world-sheet dual to line operators in various  $d$ -dimensional CFTs. An interesting case is that of the

Wilson loops in the ABJ(M) model, a prototypical example of the AdS/CFT correspondence where the  $\mathcal{N} = 6$  super Chern-Simons theory with gauge group  $U(N)_k \times U(N)_{-k}$  is conjectured to be equivalent to type IIA string theory in  $\text{AdS}_4 \times \mathbb{CP}^3$  [10].

This model admits a simple and interesting generalization [11], in which the gauge group in the Chern-Simons theory is taken to be  $U(N + \ell)_k \times U(N)_{-k}$ . In this case, the dual string theory description includes an additional flat Kalb-Ramond field, having a non-trivial holonomy on the non-contractible  $\mathbb{CP}^1 \subset \mathbb{CP}^3$ . Being the Kalb-Ramond field flat, its coupling to the open string only leads to a boundary term. As we will see in this article, the boundary term from the coupling with the Kalb-Ramond field is responsible for the materialization of the aforementioned kind of mixed boundary conditions when we study the open string dual to the 1/6 BPS *bosonic* Wilson line [12–14].

The analysis of Witten diagrams for the fluctuations on an  $\text{AdS}_2$  world-sheet enables the holographic computation of the correlation functions of some operators  $\mathcal{O}(t)$  on a line. These line correlators are related to the expectation values of local operator insertions along a Wilson line [15, 16],

$$\langle\langle \mathcal{O}(t_1) \cdots \mathcal{O}(t_n) \rangle\rangle = \langle \text{tr } \mathcal{P} [\mathcal{O}(t_1) \cdots \mathcal{O}(t_n) W_{1/6}] \rangle. \quad (1)$$

This effective theory on a line can preserve conformal symmetry at the quantum level or not, which should be reflected in the functional dependence of the correlation functions of excitations.

The main objective of our work is to test perturbatively, in inverse powers of the 't Hooft coupling, the conformal covariance of the theory on the line dual to the open string with mixed boundary conditions. In order to do that, we will analyze the functional dependence of holographic 4-point functions. For example, conformal symmetry on the line would require that the 4-point correlator of a primary field of weight  $\Delta$  has to be of the form

$$\langle\langle \mathcal{O}(t_1) \mathcal{O}(t_2) \mathcal{O}(t_3) \mathcal{O}(t_4) \rangle\rangle = \frac{G(u)}{(t_2 - t_1)^{2\Delta} (t_4 - t_3)^{2\Delta}}, \quad \text{for } u = \frac{(t_1 - t_2)(t_3 - t_4)}{(t_1 - t_3)(t_2 - t_4)}. \quad (2)$$

We will consider this for the concrete setup that corresponds to insertions in the 1/6 BPS bosonic Wilson line in the ABJ(M) model.

The paper is organized as follows. In section 2 we introduce the open string setup dual to Wilson loops in the ABJ(M) model and the possible boundary conditions on the world-sheet excitations. We show that the coupling with a flat Kalb-Ramond field leads to boundary conditions combining longitudinal and transverse derivatives and determine the propagators corresponding to them. Section 3 is dedicated to the holographic computation of 2-point and 4-point correlation functions using Witten diagrams and the propagators associated with mixed boundary conditions. Finally, in section 4 we conclude with a discussion of our results. In the appendix A we provide details about the self-energy diagrams contributing to the 1-loop correction of the propagators.

## 2 Open strings in $\text{AdS}_4 \times \mathbb{CP}^3$

We shall consider open strings embedded in  $\text{AdS}_4 \times \mathbb{CP}^3$ , whose metric can be written as

$$ds^2 = L^2 (ds_{\text{AdS}_4}^2 + 4ds_{\mathbb{CP}^3}^2), \quad (3)$$

where  $L$  is the  $\text{AdS}_4$  radius. The type IIA fields supporting this geometry are

$$e^\phi = \frac{2L}{k}, \quad F^{(4)} = \frac{3}{2} k L^2 \text{vol}(\text{AdS}_4), \quad F^{(2)} = \frac{k}{4} dA, \quad (4)$$

where  $k$  is an integer identified with the Chern-Simons level in the dual field theory, which has gauge group  $U(N)_k \times U(N)_{-k}$  [10]. Defining the 't Hooft coupling as  $\lambda = 2\pi^2 N/k$ , its relation to the  $\text{AdS}_4$

radius is  $L^2 = \sqrt{\lambda}\alpha'^{-1}$ . The 2-form  $dA$  is proportional to the Kähler form of the  $\mathbb{CP}^3$ . In angular coordinates one has

$$ds_{\mathbb{CP}^3}^2 = \frac{1}{4} \left[ d\chi^2 + \cos^2 \frac{\chi}{2} (d\theta_1^2 + \sin^2 \theta_1 d\varphi_1^2) + \sin^2 \frac{\chi}{2} (d\theta_2^2 + \sin^2 \theta_2 d\varphi_2^2) + \sin^2 \frac{\chi}{2} \cos^2 \frac{\chi}{2} (d\xi + \cos \theta_1 d\varphi_1 - \cos \theta_2 d\varphi_2)^2 \right], \quad (5)$$

with ranges  $0 \leq \chi, \theta_1, \theta_2 \leq \pi$ ,  $0 \leq \varphi_1, \varphi_2 \leq 2\pi$  and  $0 \leq \xi \leq 4\pi$  and

$$A = \cos \chi d\xi + 2 \cos^2 \frac{\chi}{2} \cos \theta_1 d\varphi_1 + 2 \sin^2 \frac{\chi}{2} \cos \theta_2 d\varphi_2. \quad (6)$$

In this background we will consider an open string ending along a straight line at the boundary of  $\text{AdS}_4$ , whose classical world-sheet is  $\text{AdS}_2$ . This gives the holographic dual description of a supersymmetric straight Wilson line in the  $\mathcal{N} = 6$  super Chern-Simons theory. It is convenient to write the (Euclidean)  $\text{AdS}_4$  metric with an explicit (Euclidean)  $\text{AdS}_2$  foliation [16]

$$ds_{\text{AdS}_4}^2 = \frac{(1 + \frac{1}{4}x^2)^2}{(1 - \frac{1}{4}x^2)^2} \left( \frac{dt^2 + dz^2}{z^2} \right) + \frac{dx^i dx^i}{(1 - \frac{1}{4}x^2)^2}. \quad (7)$$

The metric of the  $\mathbb{CP}^3$  can be parameterized alternatively in terms of 3 complex coordinates

$$ds_{\mathbb{CP}^3}^2 = \frac{d\bar{w}_a dw^a}{1 + |w|^2} - \frac{d\bar{w}_a w^a dw^b \bar{w}_b}{(1 + |w|^2)^2}. \quad (8)$$

In the static gauge  $t = \tau$  and  $z = \sigma$ , the Nambu-Goto action becomes

$$S_{\text{NG}} = \frac{\sqrt{\lambda}}{2\pi} \int d^2\sigma \sqrt{\det \left[ \frac{(1 + \frac{1}{4}x^2)^2}{(1 - \frac{1}{4}x^2)^2} g_{\mu\nu} + \frac{\partial_\mu x^i \partial_\nu x^i}{(1 - \frac{1}{4}x^2)^2} + \frac{4\partial_\mu \bar{w}_a \partial_\nu w^a}{1 + |w|^2} - \frac{4\partial_\mu \bar{w}_a w^a \partial_\nu w^b \bar{w}_b}{(1 + |w|^2)^2} \right]} \quad (9)$$

where  $g_{\mu\nu}$  is the metric of (Euclidean)  $\text{AdS}_2$

$$ds_{\text{AdS}_2}^2 = \frac{dt^2 + dz^2}{z^2}. \quad (10)$$

Expanding (9) in powers of  $x^i$  and  $w^a$ , one gets the action for 2 real scalars of mass  $m^2 = 2/L^2$  and 3 complex massless scalars respectively [18]. The dual gauge theory admits a variety of supersymmetric Wilson loops. There is a 1/6 BPS Wilson loop that involves only bosonic fields [12–14], a 1/2 BPS one [19] and even a family that interpolates between them [20–23] (see [24] for a review). These Wilson loops differ not only in the amount of supersymmetry preserved but also in their bosonic R-symmetries. For example, the symmetries of the 1/2 BPS and the 1/6 BPS bosonic Wilson loops are  $SU(3)$  and  $SU(2) \times SU(2)$  respectively. In the open string theory description, this translates into different boundary conditions on the  $\mathbb{CP}^3$  coordinates. To describe the 1/2 BPS Wilson line, Dirichlet boundary conditions must be imposed on all  $\mathbb{CP}^3$  coordinates. However, to describe the 1/6 BPS bosonic Wilson line, the string has to be uniformly smeared over a  $\mathbb{CP}^1 \subset \mathbb{CP}^3$  [12], which can be achieved by imposing Neumann boundary conditions on 2 of the  $\mathbb{CP}^3$  coordinates and Dirichlet on the rest. With this in mind, we will focus on the coordinates along a

---

<sup>1</sup>This is not the most usual convention in ABJM, but it leads to an effective string tension  $T = \frac{L^2}{2\pi\alpha'} = \frac{\sqrt{\lambda}}{2\pi}$ , which will facilitate the comparison with the  $\mathcal{N} = 4$  SYM results of [17] in the limit of Neumann boundary conditions.

particular  $\mathbb{CP}^1 \subset \mathbb{CP}^3$ , which, for the sake of definiteness, is taken to be the one given by  $\chi = 0$ , *i.e.* the one parametrized by  $\theta_1$  and  $\varphi_1$ . We can also use embedding  $\{Y^A\}$ , with  $A = 1, 2, 3$ , to describe the  $\mathbb{CP}^1$  as a surface in  $\mathbb{R}^3$  imposing  $\delta^{AB} Y^A Y^B = 1$ . Ignoring all the other transverse fluctuations, we obtain the following action for the  $\mathbb{CP}^1$  embedding coordinates

$$S_{\mathbb{CP}^1} = \frac{\sqrt{\lambda}}{2\pi} \int d^2\sigma \sqrt{\det(g_{\mu\nu} + \partial_\mu Y^A \partial_\nu Y^A)}. \quad (11)$$

The  $\mathbb{CP}^1$  fluctuations can be taken around a fix position  $n^A$ . In terms of the orthogonal part to it, one has

$$Y^A = n^A \sqrt{1 - \zeta^2} + \zeta^A, \quad (12)$$

with  $n^A \cdot \zeta^A = 0$  [17]. Thus, for small  $\zeta^A = \frac{\sqrt{2\pi}}{\lambda^{1/4}} y^A$

$$Y^A = n^A + \frac{\sqrt{2\pi}}{\lambda^{1/4}} y^A - \frac{\pi}{\sqrt{\lambda}} y^2 n^A + \mathcal{O}(\frac{1}{\lambda}), \quad (13)$$

and replacing in (11), we obtain

$$\begin{aligned} S_{\mathbb{CP}^1} = \int d^2\sigma \sqrt{g} & \left[ \frac{1}{2} \partial_\mu y^A \partial^\mu y^A + \frac{\pi}{\sqrt{\lambda}} y^A y^B \partial_\mu y^A \partial^\mu y^B + \frac{\pi}{4\sqrt{\lambda}} (\partial_\mu y^A \partial^\mu y^A)^2 \right. \\ & \left. - \frac{\pi}{2\sqrt{\lambda}} \partial_\mu y^A \partial^\mu y^B \partial_\nu y^A \partial^\nu y^B + \mathcal{O}(\frac{1}{\lambda}) \right]. \end{aligned} \quad (14)$$

This quartic action gives the vertices that play an important role in the holographic computation of 4-point correlation functions of excitations along the dual line.

## 2.1 Dirichlet, Neumann and mixed boundary conditions

Before to proceed, let us make a few comments about the boundary conditions used to specify the  $\text{AdS}_2$  propagators and their relation to the variational problem. The on-shell variation of the action (14) is, up to quadratic order, a boundary term

$$\delta S_{\mathbb{CP}^1}^{(2)} = - \int_{-\infty}^{\infty} dt \partial_z y^A \delta y^A|_{z=0}, \quad (15)$$

whose vanishing would require to set Dirichlet boundary conditions, *i.e.*  $\delta y^A|_{z=0} = 0$ . The imposition of Neumann boundary conditions would be required when another boundary term is added to the quadratic action

$$\tilde{S}_{\mathbb{CP}^1}^{(2)} = S_{\mathbb{CP}^1}^{(2)} + \int_{-\infty}^{\infty} dt \partial_z y^A y^A|_{z=0}, \quad (16)$$

so that its on-shell variation becomes

$$\delta \tilde{S}_{\mathbb{CP}^1}^{(2)} = \int_{-\infty}^{\infty} dt \delta(\partial_z y^A) y^A|_{z=0}, \quad (17)$$

whose vanishing would be achieved by demanding  $\delta(\partial_z y^A)|_{z=0} = 0$ .

In the ABJ generalization, the gauge group is  $U(N + \ell)_k \times U(N)_{-k}$ . This difference in the ranks of the gauge group factors is accounted, in the dual string theory, by incorporating a flat Kalb-Ramond field with a non-trivial holonomy on a  $\mathbb{CP}^1$  [11]<sup>2</sup>.

$$\frac{1}{2\pi} \int_{\mathbb{CP}^1} B^{(2)} = \frac{\ell}{k}, \quad B^{(2)} = \frac{\mathcal{B}}{2} dA. \quad (18)$$

Unitarity requires that  $|\ell| \leq k$  [11].

Since the Kalb-Ramond field is flat, its coupling to the open string adds just a boundary term. While the equations of motion remain unaffected, the boundary conditions on the  $\mathbb{CP}^3$  coordinates can change. To analyze this effect let us consider the expansion of the Kalb-Ramond term

$$\begin{aligned} \frac{1}{2} \frac{\sqrt{\lambda}}{2\pi} B_{\mu\nu} \epsilon^{\alpha\beta} \partial_\alpha X^\mu \partial_\beta X^\nu &= -\frac{\sqrt{\lambda}}{2\pi} \mathcal{B} \epsilon^{ABC} Y^A \partial_\tau Y^B \partial_\sigma Y^C \\ &= -\mathcal{B} \epsilon^{ABC} \left( n^A \partial_z y^B \partial_t y^C - \frac{\pi}{\sqrt{\lambda}} n^A y^2 \partial_z y^B \partial_t y^C \right. \\ &\quad \left. - \frac{2\pi}{\sqrt{\lambda}} n^C y^D \partial_t y^D y^A \partial_z y^B - \frac{2\pi}{\sqrt{\lambda}} n^B y^A y^D \partial_z y^D \partial_t y^C + \mathcal{O}\left(\frac{1}{\lambda}\right) \right). \end{aligned} \quad (19)$$

Thus, up to quadratic order

$$S_{\mathbb{CP}^1}^{(2)} = \int d^2\sigma \left( \sqrt{g} \frac{1}{2} \partial_\mu y^A \partial^\mu y^A - \mathcal{B} \epsilon^{ABC} n^A \partial_z y^B \partial_t y^C \right), \quad (20)$$

whose on-shell variation becomes

$$\delta S_{\mathbb{CP}^1}^{(2)} = - \int_{-\infty}^{\infty} dt \left( \partial_z y^A + \mathcal{B} \epsilon^{ABC} n^B \partial_t y^C \right) \delta y^A \Big|_{z=0}. \quad (21)$$

Thus, the boundary term from the coupling to the Kalb-Ramond field does not change the boundary conditions in this case, as still  $\delta y^A \Big|_{z=0} = 0$  is required. However, when the same term is added to the quadratic action which originally had Neumann boundary conditions, we get

$$\delta \tilde{S}_{\mathbb{CP}^1}^{(2)} = \int_{-\infty}^{\infty} dt \delta \left( \partial_z y^A - \mathcal{B} \epsilon^{ABC} n^B \partial_t y^C \right) y^A \Big|_{z=0}. \quad (22)$$

Therefore, in this other case the boundary conditions do get modified to

$$\delta \left( \partial_z y^A - \mathcal{B} \epsilon^{ABC} n^B \partial_t y^C \right) \Big|_{z=0} = 0. \quad (23)$$

As seen in (19), the coupling with the Kalb-Ramond field also gives rise to terms of quartic order in the orthogonal fluctuations, which will be central in the holographic computation of the 4-point functions. Using the orthogonality condition  $n^A y^A = 0$ , it is not difficult to show that these quartic terms are

$$\begin{aligned} \text{KR}^{(4)} &= \mathcal{B} \epsilon^{ABC} \left( \frac{1}{2} n^A y^2 \partial_z y^B \partial_t y^C + n^C y^D \partial_t y^D y^A \partial_z y^B + n^B y^A y^D \partial_z y^D \partial_t y^C \right) \\ &= -\mathcal{B} \epsilon^{ABC} \frac{1}{2} n^A y^2 \partial_z y^B \partial_t^C. \end{aligned} \quad (24)$$

Finally, and after a few successive integrations by parts, we obtain

$$\text{KR}^{(4)} = -\frac{\mathcal{B}}{8} \left( \partial_z \left( \epsilon^{ABC} n^A y^2 y^B \partial_t y^C \right) - \partial_t \left( \epsilon^{ABC} n^A y^2 y^B \partial_z y^C \right) \right). \quad (25)$$

---

<sup>2</sup>This  $\mathbb{CP}^1$  is not the one specified before by  $\chi = 0$  but the non-contractible 2-cycle of the  $\mathbb{CP}^3$ .

## 2.2 AdS<sub>2</sub> propagators for mixed boundary conditions

We would like to address the problem of quadratic fluctuations with specific mixed boundary conditions (23),

$$\square y^A = 0, \quad (\partial_z y^A - \mathcal{B} \epsilon^{ABC} n^B \partial_t y^C)|_{z=0} = J^A(t), \quad (26)$$

by using a suitable propagator. The free propagator for massless scalar fields in AdS<sub>2</sub> is given in terms of a Green's function

$$\langle y^A(\sigma) y^B(\sigma') \rangle_{0,n} = -G^{AB}(\sigma, \sigma'), \quad (27)$$

which is a solution of

$$\square G^{AB} = (\delta^{AB} - n^A n^B) \delta(t - t') \delta(z - z'). \quad (28)$$

The additional sub-index  $n$  in (27) serves to emphasize that the propagator depends on the values  $n^A$  chosen to compute the fluctuations. These boundary conditions are proposed to describe the string dual to the 1/6 BPS bosonic Wilson line, which is uniformly smeared over a  $\mathbb{CP}^1$ . Thus, we would have to average over the possible values of  $n^A$  eventually.

To determine the Green's function suitable for the boundary conditions (23), we can use the Green's third identity

$$y^A(z', t') = \int_{-\infty}^{\infty} dt \left( G^{AB}(z, t, z', t') \partial_z y^B(z, t) - \partial_z G^{AB}(z, t, z', t') y^B(z, t) \right) \Big|_{z=0} \quad (29)$$

and rewrite it by adding the integral of a  $t$ -derivative. We get

$$\begin{aligned} y^A(z', t') = \int_{-\infty}^{\infty} dt \Big\{ & G^{AB}(z, t, z', t') (\partial_z y^B(z, t) - \mathcal{B} \epsilon^{BCD} n^C \partial_t y^D) \\ & - (\partial_z G^{AD}(z, t, z', t') + \mathcal{B} \partial_t G^{AB}(z, t, z', t') \epsilon^{BCD} n^C) y^D \Big\} \Big|_{z=0} \end{aligned} \quad (30)$$

Thus, imposing the following boundary condition for the Green's function

$$(\partial_z G^{AD}(z, t, z', t') + \mathcal{B} \partial_t G^{AB}(z, t, z', t') \epsilon^{BCD} n^C) \Big|_{z=0} = 0, \quad (31)$$

we can easily write a solution to the problem (26) as

$$y^A(z', t') = \int_{-\infty}^{\infty} dt \left[ K^{AB}(t, z', t') (\partial_z y^B(z, t) - \mathcal{B} \epsilon^{BCD} n^C \partial_t y^D) \right] \Big|_{z=0} \quad (32)$$

where we have introduced the bulk-to-boundary propagator, obtained in this case as

$$K^{AB}(t, z', t') = \lim_{z \rightarrow 0} G^{AB}(z, t, z', t'). \quad (33)$$

At certain point, we will also consider the boundary-to-boundary propagator,

$$D^{AB}(t, t') = \lim_{z \rightarrow 0} \lim_{z' \rightarrow 0} G^{AB}(z, t, z', t'). \quad (34)$$

To proceed, we need a Green's function that satisfies (28) and (31). It is convenient to split  $G^{AB}$  into symmetric and antisymmetric parts as

$$G^{AB}(\sigma, \sigma') = (\delta^{AB} - n^A n^B) G_s(\sigma, \sigma') + \epsilon^{ABC} n^C G_a(\sigma, \sigma'). \quad (35)$$

The antisymmetric term in the propagator of the string coordinates arises from coupling the open string with the Kalb-Ramond field [25–27].

It is not difficult to see that the Green's function suitable for our problem is given by

$$G_s(\sigma, \sigma') = \frac{1}{1 - \mathcal{B}^2} G_N(\sigma, \sigma') - \frac{\mathcal{B}^2}{1 - \mathcal{B}^2} G_D(\sigma, \sigma'), \quad (36)$$

$$G_a(\sigma, \sigma') = \frac{\mathcal{B}}{1 - \mathcal{B}^2} G_0(\sigma, \sigma'), \quad (37)$$

where

$$G_N(\sigma, \sigma') = \frac{1}{4\pi} \left( \log((t - t')^2 + (z - z')^2) + \log((t - t')^2 + (z + z')^2) \right), \quad (38)$$

$$G_D(\sigma, \sigma') = \frac{1}{4\pi} \left( \log((t - t')^2 + (z - z')^2) - \log((t - t')^2 + (z + z')^2) \right), \quad (39)$$

$$G_0(\sigma, \sigma') = -\frac{1}{\pi} \tan^{-1} \left( \frac{t - t'}{z + z'} \right). \quad (40)$$

As expected, in the limit  $\mathcal{B} \rightarrow 0$ , we recover the Green's function corresponding to Neumann boundary conditions. For the bulk-to-boundary propagator we have

$$K^{AB}(z, t; t') = \frac{1}{1 - \mathcal{B}^2} (\delta^{AB} - n^A n^B) K_N(z, t; t') + \frac{\mathcal{B}}{1 - \mathcal{B}^2} \epsilon^{ABC} n^C K_0(z, t; t'), \quad (41)$$

with

$$K_N(z, t; t') = \frac{1}{2\pi} \log((t - t')^2 + z^2), \quad (42)$$

$$K_0(z, t; t') = -\frac{1}{\pi} \tan^{-1} \left( \frac{t - t'}{z} \right). \quad (43)$$

Notice that

$$\partial_t K_N = -\partial_z K_0, \quad (44)$$

and the following boundary conditions are satisfied

$$\lim_{z \rightarrow 0} \partial_z K_N(z, t; t') = \delta(t - t'), \quad \lim_{z \rightarrow 0} \partial_t K_0(z, t; t') = \delta(t - t'). \quad (45)$$

### 3 Correlators on the line from Witten diagrams on $AdS_2$

The embedding coordinates  $Y^A$  can be put in correspondence with scalar operators inserted along the Wilson line. These scalar operators should be arranged in a triplet of the  $SU(2) \subset SU(4)$ . Such triplet can be constructed using bilinears of scalars fields of the ABJ(M) theory and they are non-protected: while their scaling dimension is 1 at zero coupling, it diminishes to zero in the leading strong coupling limit. In the following, we will study correlations functions of the operators dual to embedding coordinates  $Y^A$ . We will begin with 2-point functions to read from them  $1/\sqrt{\lambda}$  corrections to the vanishing scaling dimension. Then, we will study 4-point functions to evaluate the conformal symmetry of the theory defined by this line defect.

### 3.1 2-point functions

The 1-dimensional conformal symmetry should fix the form of the 2-point correlator of embedding coordinates to be

$$\langle Y^A(t_1) Y^B(t_2) \rangle = \frac{C_Y \delta^{AB}}{(t_2 - t_1)^{2\Delta}} = C_Y \delta^{AB} \left[ 1 - \Delta L_{12} + \frac{1}{2} \Delta^2 L_{12}^2 + \dots \right], \quad (46)$$

where

$$L_{ij} := \log((t_i - t_j)^2). \quad (47)$$

The scaling dimension  $\Delta$  and normalization  $C_Y$  can be expanded at strong coupling as

$$\Delta = \frac{d_1}{\sqrt{\lambda}} + \frac{d_2}{\lambda} + \dots, \quad C_Y = c_0 + \frac{c_1}{\sqrt{\lambda}} + \frac{c_2}{\lambda} + \dots. \quad (48)$$

Thus,

$$\begin{aligned} \langle Y^A(t_1) Y^B(t_2) \rangle &= \delta^{AB} c_0 + \frac{\delta^{AB}}{\sqrt{\lambda}} (c_1 - d_1 L_{12}) \\ &\quad + \frac{\delta^{AB}}{\lambda} (c_2 - (c_0 d_2 + c_1 d_1) L_{12} + \frac{1}{2} c_0 d_1^2 L_{12}^2) + \mathcal{O}(\frac{1}{\lambda^{3/2}}). \end{aligned} \quad (49)$$

The successive orders  $c_i$  and  $d_i$  can be derived from the strong coupling expansion of this 2-point function. Using the expansion of the embedding coordinates into fluctuations around a fixed  $n^A$  (13), the leading order of the correlation function between two embedding coordinates becomes

$$\langle Y^A(t_1) Y^B(t_2) \rangle = \langle n^A n^B \rangle + \frac{2\pi}{\sqrt{\lambda}} \langle y^A(t_1) y^B(t_2) \rangle_0 + \mathcal{O}(\frac{1}{\lambda}). \quad (50)$$

Omitting the sub-index  $n$  in the brackets means that we are also averaging over  $n^A$ . Some useful averages are the following,

$$\langle n^A \rangle = 0, \quad \langle n^A n^B \rangle = \frac{1}{3} \delta^{AB}, \quad (51)$$

$$\langle n^A n^B n^C \rangle = 0, \quad \langle n^A n^B n^C n^D \rangle = \frac{1}{15} (\delta^{AB} \delta^{CD} + \delta^{AC} \delta^{BD} + \delta^{AD} \delta^{CB}). \quad (52)$$

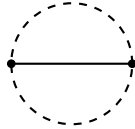


Figure 1: Contribution order  $\frac{1}{\sqrt{\lambda}}$  to  $\langle Y^A(t_1) Y^B(t_2) \rangle$

Using that the propagator (27) in the boundary-to-boundary limit becomes

$$D^{AB}(t_1, t_2) = \frac{1}{2\pi} \frac{1}{1 - \mathcal{B}^2} (\delta^{AB} - n^A n^B) \log((t_1 - t_2)^2) + \frac{1}{2} \frac{\mathcal{B}}{1 - \mathcal{B}^2} \epsilon^{ABC} n^C \text{sign}(t_2 - t_1), \quad (53)$$

we get

$$\langle Y^A(t_1) Y^B(t_2) \rangle = \frac{1}{3} \delta^{AB} \left[ 1 - \frac{2}{\sqrt{\lambda}} \frac{1}{1 - \mathcal{B}^2} \log((t_1 - t_2)^2) + \mathcal{O}(\frac{1}{\lambda}) \right]. \quad (54)$$



From this we can read that  $d_1 = \frac{2}{1-\mathcal{B}^2}$ ,  $c_0 = \frac{1}{3}$  and  $c_1 = 0$ . In other words,

$$\Delta = \frac{2}{\sqrt{\lambda}(1-\mathcal{B}^2)} + \mathcal{O}(\frac{1}{\lambda}), \quad C_Y = \frac{1}{3} + \mathcal{O}(\frac{1}{\lambda}). \quad (55)$$

To proceed beyond, we need to evaluate the 2-point function of embedding coordinates keeping track of terms order  $\frac{1}{\lambda}$ . For this we have to go further in the expansion into fluctuations around  $n^A$  (13) and also to include 1-loop corrections to the propagators,

$$\begin{aligned} \langle Y^A(t_1) Y^B(t_2) \rangle &= \frac{1}{3} \delta^{AB} \left[ 1 - \frac{2}{\sqrt{\lambda}} \frac{1}{1-\mathcal{B}^2} \log((t_1 - t_2)^2) \right] \\ &+ \frac{\pi^2}{\lambda} \langle n^A n^B y^C(t_1) y^C(t_1) y^D(t_2) y^D(t_2) \rangle_0 + \frac{2\pi}{\lambda} \langle y^A(t_1) y^B(t_2) \rangle_1 + \mathcal{O}(\frac{1}{\lambda^{3/2}}). \end{aligned} \quad (56)$$

The Witten diagrams representing the terms of the second line of (56) are depicted in Fig. 2. The

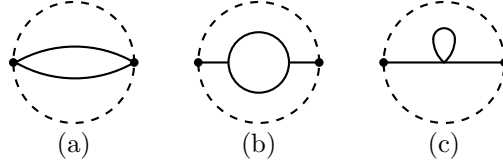


Figure 2: Contributions order  $\frac{1}{\lambda}$  to  $\langle Y^A(t_1) Y^B(t_2) \rangle$ .

first term is represented by the diagram 2(a) and its computation is rather straightforward. Before averaging over  $n^A$

$$\begin{aligned} 2(a)_n &= 2 \times \frac{\pi^2}{\lambda} n^A n^B \langle y^C(t_1) y^D(t_2) \rangle_{0,n} \langle y^C(t_1) y^D(t_2) \rangle_{0,n} \\ &= \frac{1}{\lambda} n^A n^B \frac{1}{(1-\mathcal{B}^2)^2} (L_{12}^2 + \pi^2 \mathcal{B}^2). \end{aligned} \quad (57)$$

Diagrams 2(b) and 2(c) come from the 1-loop corrections to the propagator

$$2(b)_n + 2(c)_n = \frac{2\pi}{\lambda} \langle y^A(t_1) y^B(t_2) \rangle_{1,n}. \quad (58)$$

It is possible to argue (see appendix A) that these 1-loop corrections will be of the form

$$\begin{aligned} \langle y^A(t_1) y^B(t_2) \rangle_{1,n} &= (\delta^{AB} - n^A n^B) (f_0 + f_1 L_{12} + f_2 L_{12}^2) \\ &+ \epsilon^{ABC} n^C \text{sign}(t_1 - t_2) (g_0 + g_1 L_{12}), \end{aligned} \quad (59)$$

for some constant coefficients  $f_0, f_1, f_2, g_0, g_1$ . Then, after averaging over  $n^A$ , these 3 diagrams give rise to

$$2(a) + 2(b) + 2(c) = \frac{1}{\lambda} \delta^{AB} q_{12}. \quad (60)$$

The comparison with (49) indicates that

$$q_{12} = c_2 - \frac{1}{3} d_2 L_{12} + \frac{d_1^2}{6} L_{12}^2. \quad (61)$$

In order to know the precise values of  $d_2$  and  $c_2$  one would need to compute the 1-loop corrections mentioned before. However, as we will see in the next section, these precise values would not be necessary for testing the conformal covariance of the 4-point function. For the coefficient in front of  $L_{12}^2$  to be the one indicated in (61),

$$f_2 = \frac{1}{4\pi(1 - \mathcal{B}^2)^2}, \quad (62)$$

is needed.

### 3.2 4-point functions

As stated in the Introduction, the primary goal of our article is to ascertain whether the dual theory on the line, defined by fluctuations in  $\text{AdS}_2$  with mixed boundary conditions (26), exhibits conformal behaviour. Expressing the 4-point function of embedding coordinates as

$$\langle Y^A(t_1) Y^B(t_2) Y^C(t_3) Y^D(t_4) \rangle = \frac{C_Y^2 G^{ABCD}}{(t_2 - t_1)^{2\Delta} (t_4 - t_3)^{2\Delta}}, \quad (63)$$

conformal symmetry would require that

$$G^{ABCD} = G^{ABCD}(\lambda, u), \quad (64)$$

where  $u$  is the unique independent cross-ratio

$$u = \frac{(t_1 - t_2)(t_3 - t_4)}{(t_1 - t_3)(t_2 - t_4)}. \quad (65)$$

Following [17] we can split  $G^{ABCD}$  into singlet, symmetric traceless and antisymmetric tensors

$$\begin{aligned} G^{ABCD} &= G_S \delta^{AB} \delta^{CD} + G_T (\delta^{AC} \delta^{BD} + \delta^{AD} \delta^{BC} - \frac{2}{3} \delta^{AB} \delta^{CD}) \\ &\quad + G_A (\delta^{AC} \delta^{BD} - \delta^{AD} \delta^{BC}), \end{aligned} \quad (66)$$

and concentrate on the singlet, as the other tensors can be related to  $G_S$  using crossing transformations. For  $SO(3)$ , which is the case of interest to us, one has [17]

$$G_T(u) = -\frac{3}{10} G_S(u) + \frac{9}{20} \left( u^{2\Delta} G_S\left(\frac{1}{1-u}\right) + \left(\frac{u}{1-u}\right)^{2\Delta} G_S\left(\frac{u}{1-u}\right) \right), \quad (67)$$

$$G_A(u) = \frac{3}{4} \left( u^{2\Delta} G_S\left(\frac{1}{1-u}\right) - \left(\frac{u}{1-u}\right)^{2\Delta} G_S\left(\frac{u}{1-u}\right) \right). \quad (68)$$

To compute the singlet, we just need to consider

$$\begin{aligned} \langle Y^A(t_1) Y^A(t_2) Y^B(t_3) Y^B(t_4) \rangle &= \frac{9C_Y^2 G_S(\lambda, u)}{(t_2 - t_1)^{2\Delta} (t_4 - t_3)^{2\Delta}} \\ &= 1 + \frac{Q^{(1)}}{\sqrt{\lambda}} + \frac{Q^{(2)}}{(\sqrt{\lambda})^2} + \frac{Q^{(3)}}{(\sqrt{\lambda})^3} + \mathcal{O}\left(\frac{1}{\lambda^2}\right). \end{aligned} \quad (69)$$

We can expand

$$G_S = 1 + \frac{G_S^{(1)}}{\sqrt{\lambda}} + \frac{G_S^{(2)}}{(\sqrt{\lambda})^2} + \frac{G_S^{(3)}}{(\sqrt{\lambda})^3} + \mathcal{O}\left(\frac{1}{\lambda^2}\right), \quad (70)$$

and, if each successive order is a function of the cross-ratio  $u$ , this can be regarded as an indication of the conformal symmetry of the theory on the line. To obtain the successive  $G_S^{(i)}$  one needs to compute the successive  $Q^{(i)}$ , and for this one has to use once again the expansion

$$Y^A = n^A + \frac{\sqrt{2\pi}}{\lambda^{1/4}} y^A - \frac{\pi}{\sqrt{\lambda}} y^2 n^A + \mathcal{O}\left(\frac{1}{\lambda}\right). \quad (71)$$

### Order $1/\sqrt{\lambda}$

Replacing (48) and (70) in (69), and keeping the order  $1/\sqrt{\lambda}$ , we obtain

$$G_S^{(1)} = Q^{(1)} + d_1 (L_{12} + L_{34}) . \quad (72)$$

The diagrams contributing to  $Q^{(1)}$  come from  $\langle y^A(t_1)y^A(t_2)n^B n^B \rangle_0$  and  $\langle n^A n^A y^B(t_3)y^B(t_4) \rangle_0$ , depicted in Fig. 3

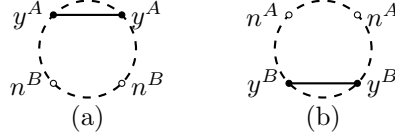


Figure 3: Diagrams contributing to  $Q^{(1)}$ .

$$3(a) = -\frac{1}{\sqrt{\lambda}} \frac{2L_{12}}{1 - \mathcal{B}^2}, \quad 3(b) = -\frac{1}{\sqrt{\lambda}} \frac{2L_{34}}{1 - \mathcal{B}^2}, \quad (73)$$

Other diagrams with just one propagator are vanishing. For example

$$\langle n^A y^A(t_2) y^B(t_3) n^B \rangle = 0 . \quad (74)$$

because  $n^A y^A = 0$ . As a consequence,

$$Q^{(1)} = -d_1 (L_{12} + L_{34}) \Rightarrow G_S^{(1)} = 0 . \quad (75)$$

### Order $1/\lambda$

Proceeding with the order  $1/\lambda$ , we obtain

$$\begin{aligned} G_S^{(2)} &= Q^{(2)} - 6c_2 + d_2 (L_{12} + L_{34}) - \frac{d_1^2}{2} (L_{12} + L_{34})^2 \\ &= Q^{(2)} - 3q_{12} - 3q_{34} - d_1^2 L_{12} L_{34}, \end{aligned} \quad (76)$$

where we have used the notation  $q_{ij}$  introduced in (61).

Let us then analyze all the diagrams contributing to  $Q^{(2)}$ . We can organize them according to the number of insertion points containing just a vector  $n^A$ , represented with a white dot in the diagrams. With  $n^A$  inserted in 2 out of the 4 points we have diagrams with either a double propagator or 1 propagator with 1-loop corrections. The diagrams in Fig. 4 are entirely analogous

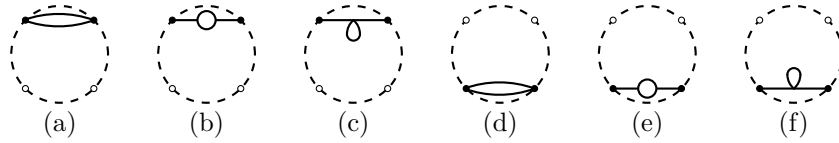


Figure 4: Some diagrams contributing to  $Q_2^{(2)}$ .

to those computing the order  $1/\lambda$  in the 2-point function. Thus

$$4(a) + 4(b) + 4(c) + 4(d) + 4(e) + 4(f) = \frac{3}{\lambda} (q_{12} + q_{34}) . \quad (77)$$

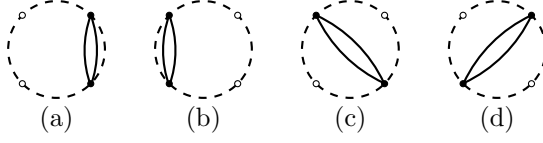


Figure 5: Some diagrams contributing to  $Q_2^{(2)}$ .

For diagrams of this sort, when contracting other pairs than 12 and 34, only the ones with the double propagator - represented in Fig. 5 - are non-vanishing. Putting all the diagrams in Fig. 4 and Fig. 5 together we obtain

$$Q_2^{(2)} = 3(q_{13} + q_{34}) + \frac{1}{(1 - \mathcal{B}^2)^2} (L_{14}^2 + L_{13}^2 + L_{23}^2 + L_{24}^2 + 4\pi^2 \mathcal{B}^2) . \quad (78)$$

Non-vanishing diagrams with just one insertion of the type  $n^A$  are shown in Fig. 6. Their total contribution is

$$Q_1^{(2)} = -\frac{2}{(1 - \mathcal{B}^2)^2} (L_{14}L_{13} + L_{23}L_{24} + L_{14}L_{23} + L_{13}L_{24}) \\ - \frac{2\pi^2 \mathcal{B}^2}{(1 - \mathcal{B}^2)^2} (S_{14}S_{13} + S_{23}S_{24} + S_{14}S_{23} + S_{13}S_{24}) , \quad (79)$$

where

$$S_{ij} := \text{sign}(t_i - t_j) . \quad (80)$$

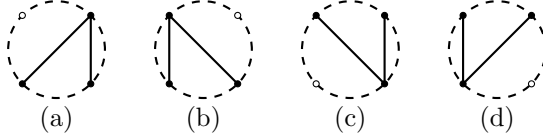


Figure 6: Diagrams contributing to  $Q_1^{(2)}$ .

The last contribution to this order comes from diagrams with  $y^A$  in the 4 insertion points, as represented in Fig. 7. They give

$$Q_0^{(2)} = \frac{1}{(1 - \mathcal{B}^2)^2} (4L_{12}L_{34} + 2L_{14}L_{23} + 2\pi^2 \mathcal{B}^2 S_{14}S_{23} + 2L_{13}L_{24} + 2\pi^2 \mathcal{B}^2 S_{13}S_{24}) . \quad (81)$$

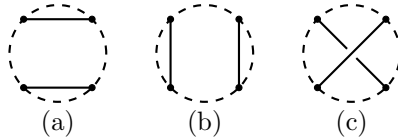


Figure 7: Diagrams contributing to  $Q_0^{(2)}$ .

Now, we can combine all the contributions to  $Q^{(2)}$ . Note that the terms proportional to  $q_{12}$ ,  $q_{34}$  and  $L_{12}L_{34}$  in the rhs of (76) cancel with some of the contributions to  $Q^{(2)}$ . As a result, we obtain the following expression for  $G_S^{(2)}$

$$G_S^{(2)} = \frac{1}{(1 - \mathcal{B}^2)^2} (L_{14} + L_{23} - L_{13} - L_{24})^2 + \frac{\pi^2 \mathcal{B}^2}{(1 - \mathcal{B}^2)^2} (S_{14} + S_{23} - S_{13} - S_{24})^2, \quad (82)$$

which can be re-expressed as a function of the cross-ratio

$$G_S^{(2)}(u) = \frac{4}{(1 - \mathcal{B}^2)^2} [\log^2(1 - u) + \pi^2 \mathcal{B}^2 \Theta(u - 1)], \quad (83)$$

where  $\Theta$  is the Heaviside step function. The fact that the first non-trivial contribution to  $G_S$  is indeed just a function of the cross-ratio serves as evidence for the conformal covariance of the 4-point function. Another interesting observation about this result is that it verifies

$$G_S^{(2)}(u) = G_S^{(2)}\left(\frac{u}{u-1}\right), \quad (84)$$

a crossing symmetry relation from the exchange  $t_3 \longleftrightarrow t_4$ .

It is worth noting that, at this order, all contributions arise from reducible diagrams originated from quadratic terms in the action of fluctuations. A more robust confirmation of conformal covariance would be obtained exploring the next order, which incorporates contributions from connected Witten diagrams involving quartic terms.

### Order $1/(\sqrt{\lambda})^3$

Expanding eq. (69) to order  $\frac{1}{\lambda^{3/2}}$ , we obtain

$$G_S^{(3)} = Q^{(3)} - 6c_3 + \left(d_3 + 6d_1c_2 + d_1G_S^{(2)}\right)(L_{12} + L_{34}) - d_1d_2(L_{12} + L_{34})^2 + \frac{d_1^3}{6}(L_{12} + L_{34})^3. \quad (85)$$

At this order we will have to include irreducible diagrams from the quartic terms of the action contributing to  $Q^{(3)}$ , like the one depicted in Fig. 8. There are 4 different types of quartic vertices

$$V_1 = \frac{\pi}{\sqrt{\lambda}} y^A y^B \partial_\mu y^A \partial^\mu y^B, \quad V_2 = \frac{\pi}{4\sqrt{\lambda}} (\partial_\mu y^A \partial^\mu y^A)^2, \quad (86)$$

$$V_3 = -\frac{\pi}{2\sqrt{\lambda}} \partial_\mu y^A \partial^\mu y^B \partial_\nu y^A \partial^\nu y^B, \quad V_4 = -\frac{\pi}{\sqrt{\lambda}} \frac{1}{\sqrt{g}} \mathcal{B} \epsilon^{ABC} n^A y^2 \partial_z y^B \partial_t y^C. \quad (87)$$

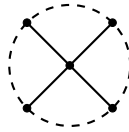


Figure 8: Irreducible diagrams contributing to  $Q^{(3)}$ .

All these diagrams involve a spacetime integration of products of bulk-to-boundary propagators. The diagram with  $V_1$  will be more intricate, as two propagators, appearing without derivatives, introduce logarithmic or arc tangent factors. To avoid this complication, we can compute

$\partial_{t_1}\partial_{t_2}\partial_{t_3}\partial_{t_4}\langle Y^A(t_1)Y^A(t_2)Y^B(t_3)Y^B(t_4)\rangle$ . Therefore, instead of (85), we will consider

$$\begin{aligned}\partial_{t_1}\partial_{t_2}\partial_{t_3}\partial_{t_4}G_S^{(3)} &= \partial_{t_1}\partial_{t_2}\partial_{t_3}\partial_{t_4}Q^{(3)} + d_1\partial_{t_1}\partial_{t_2}\partial_{t_3}\partial_{t_4}\left(G_S^{(2)}(L_{12}+L_{34})\right) \\ &\quad - 2d_1d_2\partial_{t_1}\partial_{t_2}\partial_{t_3}\partial_{t_4}(L_{12}L_{34}) + \frac{d_1^3}{2}\partial_{t_1}\partial_{t_2}\partial_{t_3}\partial_{t_4}(L_{12}^2L_{34}+L_{12}L_{34}^2). \quad (88)\end{aligned}$$

It is straightforward to check that, acting with the four derivatives on a function of the cross-ratio, we obtain<sup>3</sup>

$$\partial_{t_1}\partial_{t_2}\partial_{t_3}\partial_{t_4}F(u) = \frac{\tilde{F}(u)}{(t_1-t_2)^2(t_3-t_4)^2}. \quad (89)$$

Therefore, we have to check whether the rhs of (88) is of this form.

Let us begin by computing the irreducible contact diagrams. For the vertex  $V_1$  we have to compute

$$\partial_{t_1}\partial_{t_2}\partial_{t_3}\partial_{t_4}Q_{irred,1}^{(3)} = -4\pi^3 \int d^2\sigma \sqrt{g} \langle \partial_{t_1}y^A \partial_{t_2}y^A \partial_{t_3}y^B \partial_{t_4}y^B y^C y^D \partial_\mu y^C \partial^\mu y^D \rangle_0. \quad (90)$$

This can be explicitly computed and the result is

$$\begin{aligned}t_{12}^2 t_{34}^2 \partial_{t_1}\partial_{t_2}\partial_{t_3}\partial_{t_4}Q_{irred,1}^{(3)} &= -\frac{8u^2[u(u-2)+2]\log(u)}{(1-\mathcal{B}^2)^2(1-u)^2} + \frac{8u^2\log(1-u)}{(1-\mathcal{B}^2)^2} - \frac{8u^2}{(1-\mathcal{B}^2)^2(1-u)} \\ &\quad - \frac{32t_{12}^2 t_{34}^2}{(1-\mathcal{B}^2)^3} \left( \frac{1}{t_{12}t_{23}t_{24}} - \frac{1}{t_{12}t_{13}t_{14}} \right) - \frac{16(3-\mathcal{B}^2)}{(1-\mathcal{B}^2)^4} t_{12}^2 t_{34}^2 \left( \frac{1}{t_{12}t_{23}t_{24}^2} - \frac{1}{t_{12}t_{13}t_{14}^2} \right) \\ &\quad - 16 \frac{(1+\mathcal{B}^2)}{(1-\mathcal{B}^2)^4} t_{12}^2 t_{34}^2 \left( \frac{1}{t_{13}t_{23}t_{34}} + \frac{1}{t_{13}t_{23}t_{34}} - \frac{1}{t_{12}^2 t_{23}t_{24}} - \frac{1}{t_{12}^2 t_{13}t_{14}} - \frac{2}{t_{13}t_{23}t_{34}^2} \right). \quad (91)\end{aligned}$$

One comment is in order about this result. As we have assumed that all  $t_i$  are different to perform the integrals, we have lost track of contact-like terms in the form of Dirac deltas or derivatives of them. We know this type of terms appear in the reducible diagrams, from derivatives acting on the sign functions present in the boundary-to-boundary propagators.

In relation with our motivation for the study of this 4-point function, we should notice the appearance of terms that are not functions of the cross-ratio. Similar anomalous contributions appear in the vertex originated from the coupling with the Kalb-Ramond field

$$\partial_{t_1}\partial_{t_2}\partial_{t_3}\partial_{t_4}Q_{irred,4}^{(3)} = 4\pi^3 \mathcal{B} n^C \epsilon^{CDE} \int d^2\sigma \langle \partial_{t_1}y^A \partial_{t_2}y^A \partial_{t_3}y^B \partial_{t_4}y^B y^F y^F \partial_z y^D \partial_t y^E \rangle_0. \quad (92)$$

The remaining irreducible contributions are not anomalous, *i.e.*  $t_{12}^2 t_{34}^2 \partial_{t_1}\partial_{t_2}\partial_{t_3}\partial_{t_4}Q_{irred,2}^{(3)}$  and  $t_{12}^2 t_{34}^2 \partial_{t_1}\partial_{t_2}\partial_{t_3}\partial_{t_4}Q_{irred,3}^{(3)}$  are just functions of the cross-ratio.

---

<sup>3</sup>Where

$$\tilde{F}(u) = u^2 \left[ u^2(u-1)^2 F^{(4)}(u) + 4u(u-1)(2u-1)F^{(3)}(u) + (2+14u(u-1))F''(u) + 2u^2(2u-1)F'(u) \right].$$

Collecting all the irreducible diagrams we have

$$\begin{aligned}
t_{12}^2 t_{34}^2 \partial_{t_1} \partial_{t_2} \partial_{t_3} \partial_{t_4} Q_{irred}^{(3)} &= \frac{8(4 - 8u + 7u^2 - 3u^3 + 2u^4)}{(1 - \mathcal{B}^2)^2(1 - u)^2} + \frac{16(2 - u + u^4) \log(1 - u)}{(1 - \mathcal{B}^2)^2 u} \\
&\quad - \frac{16u^4(3 - 3u + u^2) \log(u)}{(1 - \mathcal{B}^2)^2(1 - u)^3} \\
&\quad - \frac{16t_{12}^2 t_{34}^2}{(1 - \mathcal{B}^2)^3} \left( \frac{3}{t_{12} t_{23} t_{24}^2} - \frac{3}{t_{12} t_{13} t_{14}^2} + \frac{2}{t_{12} t_{23}^2 t_{24}} - \frac{2}{t_{12} t_{13}^2 t_{14}} - \frac{2}{t_{13} t_{23} t_{34}^2} \right. \\
&\quad \left. + \frac{1}{t_{13} t_{23}^2 t_{34}} + \frac{1}{t_{13}^2 t_{23} t_{34}} - \frac{1}{t_{12}^2 t_{13} t_{14}} - \frac{1}{t_{12}^2 t_{23} t_{24}} \right). \tag{93}
\end{aligned}$$

It is worth noting that the coefficient in front of the anomalous terms becomes  $(1 - \mathcal{B}^2)^{-3}$  after collecting all irreducible diagrams. This is in principle a good sign, as other contributions that can potentially cancel these anomalous terms could only come from reducible diagrams with just three propagators.

We now turn to reducible diagrams contributing to  $Q^{(3)}$ . We can distinguish two kinds of reducible contributions: diagrams with just 3 free propagators and diagrams with 2 propagators, one of them being 1-loop corrected. These diagrams are represented in Fig. 9 and Fig. 10 respectively<sup>4</sup>.

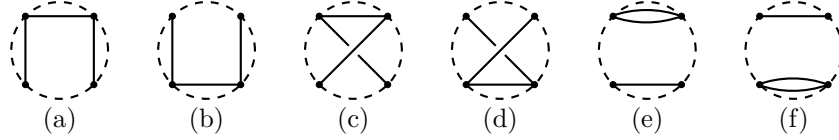


Figure 9: Diagrams contributing to  $\partial_{t_1} \partial_{t_2} \partial_{t_3} \partial_{t_4} Q_{red,0}^{(3)}$ .

Summing diagrams with 3 propagators we find

$$\begin{aligned}
\partial_{t_1} \partial_{t_2} \partial_{t_3} \partial_{t_4} Q_{red,0}^{(3)} &= \frac{16}{(1 - \mathcal{B}^2)^3} \left[ -\frac{1}{t_{12} t_{23} t_{14}^2} + \frac{1}{t_{12} t_{23}^2 t_{14}} - \frac{1}{t_{12}^2 t_{23} t_{14}} + \frac{1}{t_{12} t_{13} t_{24}^2} - \frac{1}{t_{12} t_{13}^2 t_{24}} \right. \\
&\quad - \frac{1}{t_{12}^2 t_{13} t_{24}} + \frac{4}{t_{12}^2 t_{34}^2} - \frac{1}{t_{23} t_{14} t_{34}^2} - \frac{1}{t_{13} t_{24} t_{34}^2} - \frac{1}{t_{23} t_{14}^2 t_{34}} + \frac{1}{t_{23}^2 t_{14} t_{34}} - \frac{1}{t_{13} t_{24}^2 t_{34}} \\
&\quad \left. + \frac{1}{t_{13}^2 t_{24} t_{34}} - \frac{1}{2} \left( \frac{1}{t_{23}^2 t_{14}^2} + \frac{1}{t_{13}^2 t_{24}^2} + \frac{2}{t_{12}^2 t_{34}^2} \right) (L_{12} + L_{34}) \right]. \tag{94}
\end{aligned}$$

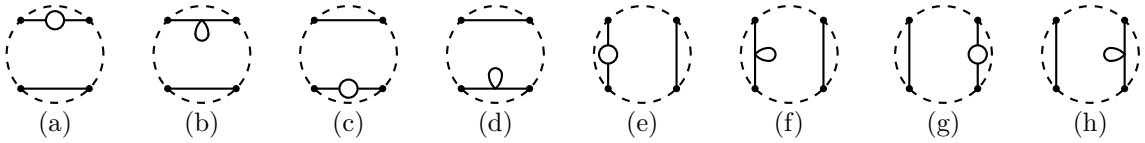


Figure 10: Diagrams contributing to  $\partial_{t_1} \partial_{t_2} \partial_{t_3} \partial_{t_4} Q_{red,1}^{(3)}$ .

<sup>4</sup>There are more diagrams of these types. In Fig. 9 and Fig. 10 we show only those non-vanishing after taking the derivatives with respect to the position of the insertion points.

For the diagrams in Fig. 10, with one of propagators corrected at the 1-loop level, we can use the 2-point function (59) used in section 3.1. We obtain

$$\partial_{t_1} \partial_{t_2} \partial_{t_3} \partial_{t_4} Q_{red,1}^{(3)} = -\frac{32\pi}{(1-\mathcal{B}^2)} \left[ (f_1 - 4f_2) \left( \frac{1}{t_{23}^2 t_{14}^2} + \frac{1}{t_{13}^2 t_{24}^2} + \frac{2}{t_{12}^2 t_{34}^2} \right) + f_2 \left( \frac{L_{23} + L_{14}}{t_{23}^2 t_{14}^2} + \frac{L_{13} + L_{24}}{t_{13}^2 t_{24}^2} + \frac{2L_{12} + 2L_{34}}{t_{12}^2 t_{34}^2} \right) \right]. \quad (95)$$

We will use, as we have argued in section 3.1, that  $f_2 = \frac{1}{4\pi(1-\mathcal{B}^2)^2}$ , but the coefficient  $f_1$  will remain indeterminate.

Having computed all the diagrammatic contributions enclosed in  $\partial_{t_1} \partial_{t_2} \partial_{t_3} \partial_{t_4} Q^{(3)}$ , it remains to consider the last three terms in (88), which give

$$\begin{aligned} d_1 \partial_{t_1} \partial_{t_2} \partial_{t_3} \partial_{t_4} \left( G_S^{(2)} (L_{12} + L_{34}) \right) &= \frac{32}{(1-\mathcal{B}^2)^3} \left[ -\frac{1}{t_{12} t_{13} t_{14}^2} + \frac{1}{t_{12} t_{23} t_{14}^2} - \frac{1}{t_{12} t_{13}^2 t_{14}} - \frac{1}{t_{12}^2 t_{13} t_{14}} \right. \\ &\quad - \frac{1}{t_{12} t_{23}^2 t_{14}} + \frac{1}{t_{12}^2 t_{23} t_{14}} - \frac{1}{t_{12} t_{13} t_{24}^2} + \frac{1}{t_{12} t_{23} t_{24}^2} + \frac{1}{t_{12} t_{13}^2 t_{24}} \\ &\quad + \frac{1}{t_{12}^2 t_{13} t_{24}} + \frac{1}{t_{12} t_{23}^2 t_{24}} - \frac{1}{t_{12}^2 t_{23} t_{24}} - \frac{1}{t_{13} t_{23} t_{34}^2} + \frac{1}{t_{23} t_{14} t_{34}^2} \\ &\quad + \frac{1}{t_{13} t_{24} t_{34}^2} - \frac{1}{t_{14} t_{24} t_{34}^2} + \frac{1}{t_{13} t_{23}^2 t_{34}} + \frac{1}{t_{13}^2 t_{23} t_{34}} + \frac{1}{t_{23} t_{14}^2 t_{34}} \\ &\quad - \frac{1}{t_{23}^2 t_{14} t_{34}} + \frac{1}{t_{13} t_{24}^2 t_{34}} - \frac{1}{t_{14} t_{24}^2 t_{34}} - \frac{1}{t_{13}^2 t_{24} t_{34}} - \frac{1}{t_{14}^2 t_{24} t_{34}} \\ &\quad \left. + \frac{1}{2} \left( \frac{1}{t_{13}^2 t_{24}^2} + \frac{1}{t_{14}^2 t_{23}^2} \right) (L_{12} + L_{34}) \right], \quad (96) \end{aligned}$$

$$2d_1 d_2 \partial_{t_1} \partial_{t_2} \partial_{t_3} \partial_{t_4} (L_{12} L_{34}) = \frac{16d_2}{(1-\mathcal{B}^2)} \frac{1}{t_{12}^2 t_{34}^2}, \quad (97)$$

$$\frac{d_1^3}{2} \partial_{t_1} \partial_{t_2} \partial_{t_3} \partial_{t_4} (L_{12}^2 L_{34} + L_{12} L_{34}^2) = -\frac{128}{(1-\mathcal{B}^2)^3} \frac{1}{t_{12}^2 t_{34}^2} + \frac{32}{(1-\mathcal{B}^2)^3} \frac{(L_{12} + L_{34})}{t_{12}^2 t_{34}^2}. \quad (98)$$

We are in a position to collect all the contributions to  $\partial_{t_1} \partial_{t_2} \partial_{t_3} \partial_{t_4} G_S^{(3)}$  and analyze its dependence on  $t_1, t_2, t_3$  and  $t_4$ . The final result can be simply expressed as follows:

$$t_{12}^2 t_{34}^2 \partial_{t_1} \partial_{t_2} \partial_{t_3} \partial_{t_4} G_S^{(3)} = P(u) + P\left(\frac{u}{u-1}\right), \quad (99)$$

where

$$\begin{aligned} P(u) &= -\frac{8u^2}{(1-\mathcal{B}^2)^3} [4 + \log(u^2)] + \frac{8}{(1-\mathcal{B}^2)^2} \left[ 2 + u + 2u^2 + \left( \frac{2}{u} - 1 + \frac{u^3}{(1-u)^3} \right) \log(u^2) \right] \\ &\quad + \frac{8}{(1-\mathcal{B}^2)} [-d_2 + 32\pi f_1 (1 + u^2)]. \quad (100) \end{aligned}$$

As anticipated and in accordance with the conformal symmetry of the line, we observe that the anomalous terms cancel and this is a function of the cross-ratio. Furthermore, crossing symmetry resulting from the exchange between  $t_3$  and  $t_4$  is evident in (99) as well.

It is noteworthy to mention the appearance of indeterminate coefficients, such as those in (95) and (97). In fact, in the case of  $f_2$ , the use of the specific value given in section 3.1 is crucial for arranging  $L_{ij}$  terms into a function of  $u$ . Conversely, the terms with  $f_1$  and  $d_2$  lead to functions of the cross-ratio for any value of these coefficients.



## 4 Discussion

The type IIA background for the dual description of the ABJ(M) model -  $\text{AdS}_4 \times \mathbb{CP}^3$  - includes a flat Kalb-Ramond field that couples to the string through a boundary term. Therefore, this can affect the boundary conditions of an open string dual to a Wilson loop in the gauge theory. For the case of a straight Wilson line, the dual open string has an  $\text{AdS}_2$  world-sheet ending along a line at the boundary of  $\text{AdS}_4$ . In accordance with the symmetries of 1/6 BPS bosonic Wilson line, the dual open string satisfies certain boundary condition that delocalizes it around a  $\mathbb{CP}^1 \subset \mathbb{CP}^3$  [12]. One of the main observations of our work is that the fluctuations on the open string dual to the 1/6 BPS bosonic Wilson line in the ABJ(M) model satisfy some boundary conditions mixing longitudinal and transverse derivatives, where the mixing parameter comes from the Kalb-Ramond field. Thus, the Neumann boundary condition - the vanishing of the derivative transverse to the boundary - proposed to describe the smearing of the dual string over a  $\mathbb{CP}^1 \subset \mathbb{CP}^3$  [28] would be appropriate for the ABJM model, when the two gauge group factors of the Chern-Simons theory has equal ranks. In the ABJ(M) generalization, when the two gauge group factors are different, the open string dual to 1/6 BPS bosonic Wilson loops becomes delocalized around a  $\mathbb{CP}^1 \subset \mathbb{CP}^3$  using mixed boundary conditions instead. This constitutes another concrete realization of the supersymmetric mixed boundary conditions (invariant under 4 supercharges) proposed in [9].

Using scalar fields with these mixed boundary conditions in the  $\text{AdS}_2$  world-sheet, we have holographically computed correlation functions of excitations along the 1/6 BPS bosonic Wilson line in the ABJ(M) model. As evidenced by the fact that the quantity (99) is a function of the cross-ratio, a 1/6 BPS bosonic Wilson line with local operator insertions in the ABJ(M) model constitutes a  $\text{CFT}_1$ . This result is significant because, being the theory on the line a  $\text{CFT}_1$ , it would be possible to use analytic bootstrap techniques to investigate its correlation functions, extending the analysis conducted in [18]. An important difference in the present case is that, despite the supersymmetry of the Wilson loop, some of the fluctuations are not part of protected multiplets and receive corrections to their scaling dimensions. Bootstrap techniques have been shown to be powerful when used in combination with integrability to study Wilson loops in  $\mathcal{N} = 4$  super Yang-Mills [29–33]. In the present realization of the AdS/CFT correspondence, integrability has been observed for 1/2 BPS Wilson loops in the ABJM setup [34]. It would be therefore interesting to explore the integrability for 1/6 BPS Wilson loops in the ABJ(M) model, bearing in mind that the coupling with the Kalb-Ramond field breaks the parity symmetry in the dual line. Some results of integrability in ABJ theories for closed spin chains can be found for example in [35] and references therein.

The mixing boundary conditions we discussed in this article resemble a type of boundary conditions discussed in [36]. More concretely, the boundary conditions here are similar to the  $t$ -derivative of the boundary conditions there. However, in that case, as presented in [36], the 4-point function does not have the form expected for a conformal field theory. In the current case, a key difference is the fact that the boundary conditions describe a smeared string configuration. This has prompted us to consider orthogonal fluctuations to embedding coordinates. As a result, additional reducible diagram contributions have to be included, which are ultimately the ones cancelling the anomalous terms originated from quartic vertices irreducible diagrams. It is important to emphasize that, while the boundary conditions considered in [9] and [36] were regarded as candidates for the dual string to the interpolating family of Wilson loops [20–23], in this current article the boundary conditions we discuss account for the 1/6 BPS bosonic Wilson loops in the ABJ(M) generalization of the model.

Another interesting problem for the future would be the inclusion of Green-Schwarz fermions in the world-sheet, to determine their boundary conditions and to compute fermionic 1-loop Witten diagrams. This would enable a thorough derivation of the 1-loop correction to the propagator in a detailed fashion. This would be important to validate the form we have proposed in (59) and

ascertain the value for the coefficient  $f_2$  in (62), which was crucial for the conformal covariance of both, the 2-point and the 4-point function. Furthermore, one would be able to explicitly determine the coefficients  $f_1$  and  $d_2$  that appear in the 4-point function and give the anomalous dimension to the next perturbative order.

## Acknowledgments

We thank Alberto Faraggi, Martín Lagares and Guillermo Silva for discussion and comments. This work was partially supported by PICT 2020-03749, PIP 02229 and UNLP X910. DHC would like to acknowledge support from the ICTP through the Associates Programme (2020-2025) during the initial stages of this project.

## A Self-energy corrections to the propagator

Previously, we have used that the 1-loop correction to the 2-point function takes the form,

$$\langle y^A(t_1)y^B(t_2) \rangle_{1,n} = (\delta^{AB} - n^A n^B) (f_0 + f_1 L_{12} + f_2 L_{12}^2) + \epsilon^{ABC} n^C S_{12} (g_0 + g_1 L_{12}) . \quad (101)$$

It is possible to study loop diagram contributions to determine whether (101) is a reasonable assumption or not. There are two types of diagrams contributing to the 1-loop correction of the propagator, as shown in Fig. 11. We will briefly analyze the functions obtained from diagrams of the *self-energy* type represented by Fig. 11 (b), but diagrams 11 (a), corresponding to *fermionic loops* (and harder to compute), will not be considered in this appendix. Therefore, this analysis will be focused on verifying the type of functions appearing in (101) rather than determining the values of the coefficients  $f_0$ ,  $f_1$ ,  $f_2$ ,  $g_0$  and  $g_1$ .

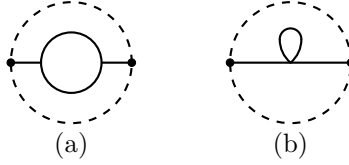


Figure 11: Contributions to  $\langle y^A(t_1)y^B(t_2) \rangle_{1,n}$ .

Let us then concentrate on self-energy diagrams like the one in 11(b),

$$\begin{aligned} 11(b)_n &= - \int d^2\sigma \sqrt{g} \langle y^A(t_1) \hat{V}(\tau, \sigma) y^B(t_2) \rangle \\ &= (\delta^{AB} - n^A n^B) \Pi(t_{12}) + \epsilon^{ABC} n^C \Xi(t_{12}) , \end{aligned} \quad (102)$$

where  $\hat{V}(\tau, \sigma)$  represents all the quartic terms in the expansion of the Nambu-Goto-Kalb-Ramond action (86)-(87). The different contributions from each type of vertex depend on which fields are contracted into a tadpole. This will lead to propagators evaluated at coincident points, which have to be regularized to remove UV divergences from them. To this end we can deform  $G_s$  with a covariant UV cutoff

$$G_s(\sigma, \sigma') = \frac{1}{4\pi} \log((t - t')^2 + (z - z')^2 + \varepsilon^2 z z') + \frac{1}{4\pi} \frac{1 + \mathcal{B}^2}{1 - \mathcal{B}^2} \log((t - t')^2 + (z + z')^2) , \quad (103)$$

and from this

$$\lim_{\sigma' \rightarrow \sigma} G_s(\sigma, \sigma') = \frac{1}{2\pi} \log(2\varepsilon) + \frac{1}{\pi} \frac{1}{1 - \mathcal{B}^2} \log z, \quad (104)$$

$$\lim_{\sigma' \rightarrow \sigma} \partial_z G_s(\sigma, \sigma') = \frac{1}{2\pi z} \frac{1}{1 - \mathcal{B}^2}. \quad (105)$$

The dependence with the cutoff  $\varepsilon$  should cancel once the fermionic loop contribution is included [17]. The double-derivative of  $G_s$  in the coincidence limit is a bit more subtle, as it typically depends on the regularization scheme [37]. A natural choice is to use a scheme that preserves the symmetries of the background [38]. In the case of Neumann boundary conditions propagator, this choice leads to [17]

$$\begin{aligned} \lim_{\sigma' \rightarrow \sigma} \partial_\mu \partial^{\mu'} G_N(\sigma, \sigma') &= \frac{1}{4\pi} \lim_{\sigma' \rightarrow \sigma} \partial_\mu \partial^{\mu'} [\log((t - t')^2 + (z - z')^2) + \log((t - t')^2 + (z + z')^2)] \\ &= -\frac{1}{2\pi}. \end{aligned} \quad (106)$$

The second term in this limit is regular and  $\lim_{\sigma' \rightarrow \sigma} \partial_\mu \partial^{\mu'} \log((t - t')^2 + (z + z')^2) = -1$ . This means that the choice made in (106) implies that  $\lim_{\sigma' \rightarrow \sigma} \partial_\mu \partial^{\mu'} \log((t - t')^2 + (z - z')^2) = -1$ . This, in turn, leads to

$$\lim_{\sigma' \rightarrow \sigma} \partial_\mu \partial^{\mu'} G_s(\sigma, \sigma') = -\frac{1}{2\pi} \frac{1}{1 - \mathcal{B}^2}. \quad (107)$$

Let us present, with some detail, the following contribution from  $V_1$ ,

$$\begin{aligned} -\frac{2\pi}{\sqrt{\lambda}} \int \frac{d^2\sigma}{z^2} \langle (\overline{y^C} y^D \partial_\mu \overline{y^C} \partial^\mu \overline{y^D}) y^A(t_1) y^B(t_2) \rangle &= \frac{2}{\sqrt{\lambda}} \frac{1}{1 - \mathcal{B}^2} \int \frac{d^2\sigma}{z^2} \log z \partial_\mu K^{CA} \partial^\mu K^{CB} \\ &= \frac{2}{\sqrt{\lambda}} \frac{1}{(1 - \mathcal{B}^2)^3} [(\delta^{AB} - n^A n^B) I_1 + \mathcal{B} \epsilon^{ABC} n^C I_2] \end{aligned} \quad (108)$$

where we have omitted the  $\log \varepsilon$  term. The integrals  $I_1$  and  $I_2$ , up to constants and IR divergences, are<sup>5</sup>

$$I_1 = \int \frac{d^2\sigma}{z^2} \log z (\partial_\mu K_N(t_1) \partial^\mu K_N(t_2) + \mathcal{B}^2 \partial_\mu K_0(t_1) \partial^\mu K_0(t_2)) = \frac{(1 + \mathcal{B}^2)}{8\pi} (\log 16 L_{12} - L_{12}^2) \quad (109)$$

$$I_2 = \int \frac{d^2\sigma}{z^2} \log z (\partial_\mu K_N(t_1) \partial^\mu K_0(t_2) - \partial_\mu K_0(t_1) \partial^\mu K_N(t_2)) = \frac{1}{2} S_{12} (L_{12} - \log 4). \quad (110)$$

From this single contribution, we already observe the appearance of terms of the form presented in (101). Since we will not consider the fermionic loop contributions here, keeping track of all the self-energy contributions with plenty of details would not be particularly illuminating. Nonetheless, considering the conformal covariance verification we perform in this article depends on the actual value of the coefficient  $f_2$ , it might be worthwhile to collect all the contributions of the form  $L_{12}^2$ .

In addition to the one from (108)-(109), other contributions from this vertex to  $\Pi$  arise with the coincidence-limit factors (105), (107) and (111)

$$\lim_{\sigma' \rightarrow \sigma} \partial_t G_a(\sigma, \sigma') = -\frac{1}{2\pi z} \frac{\mathcal{B}}{1 - \mathcal{B}^2}. \quad (111)$$

---

<sup>5</sup>In the following,  $K_{N/0}(t_i)$  stands for  $K_{N/0}(z, t; t_i)$ .

Collecting all of them

$$\Pi_1 = \frac{1}{\sqrt{\lambda}} \left( \frac{2I_1}{(1-\mathcal{B}^2)^3} + \frac{6I_3}{(1-\mathcal{B}^2)^3} - \frac{I_4}{(1-\mathcal{B}^2)^3} - \frac{2\mathcal{B}^2 I_5}{(1-\mathcal{B}^2)^3} \right), \quad (112)$$

where now

$$I_3 = \int \frac{d^2\sigma}{z} (K_N(t_1)\partial_z K_N(t_2) + \mathcal{B}^2 K_0(t_1)\partial_z K_0(t_2)) = \frac{(1+\mathcal{B}^2)}{8\pi} L_{12}^2, \quad (113)$$

$$I_4 = \int \frac{d^2\sigma}{z^2} (K_N(t_1)K_N(t_2) + \mathcal{B}^2 K_0(t_1)K_0(t_2)) = \frac{(1+\mathcal{B}^2)}{4\pi} (L_{12}^2 + 4L_{12}), \quad (114)$$

$$I_5 = \int \frac{d^2\sigma}{z} (K_N(t_1)\partial_t K_0(t_2) - K_0(t_1)\partial_t K_N(t_2)) = \frac{1}{4\pi} L_{12}^2. \quad (115)$$

These contributions come from different Wick contractions of the vertex  $V_1$ . The  $I_3$  and  $I_5$  terms comes from  $\langle (\overbrace{y^C y^D \partial_\mu y^C \partial^\mu y^D}) y^A(t_1) y^B(t_2) \rangle$  and  $\langle (\overbrace{y^C y^D \partial_\mu y^C \partial^\mu y^D}) y^A(t_1) y^B(t_2) \rangle$ , while the  $I_4$  term comes from  $\langle y^A(t_1) y^B(t_2) (\overbrace{y^C y^D \partial_\mu y^C \partial^\mu y^D}) \rangle$ .

Finally, we find

$$\begin{aligned} \Pi_1 &= \frac{1}{\sqrt{\lambda}} \frac{1}{8\pi} \frac{(1+\mathcal{B}^2)}{(1-\mathcal{B}^2)^3} (-2+6-2) L_{12}^2 - \frac{1}{2\pi} \frac{\mathcal{B}^2}{(1-\mathcal{B}^2)^3} L_{12}^2 + \dots \\ &= \frac{1}{4\pi} \frac{1}{(1-\mathcal{B}^2)^2} L_{12}^2 + \dots, \end{aligned} \quad (116)$$

where the ellipsis represents the omission of  $L_{12}$  and constant terms.

We shall not discuss in detail the contributions to  $\Pi$  from vertices  $V_2$  and  $V_3$  with 4 derivatives, nor from vertices  $\partial x^i \partial x^i \partial y^C \partial y^C$ , as it is straightforward to check that they contribute to the  $L_{12}$  but not to the  $L_{12}^2$  dependence. Other contributions to  $\Pi$  could arise from  $V_4$ , originated from the coupling with the Kalb-Ramond field. For these other contributions, in addition to (104) and (105), we will also need the following propagators in the coincidence limit

$$\lim_{\sigma' \rightarrow \sigma} \partial_t \partial_{z'} G_a(\sigma, \sigma') = \frac{1}{4\pi z^2} \frac{\mathcal{B}}{1-\mathcal{B}^2}, \quad (117)$$

$$\lim_{\sigma' \rightarrow \sigma} \partial_t G_a(\sigma, \sigma') = -\frac{1}{2\pi z} \frac{\mathcal{B}}{1-\mathcal{B}^2}, \quad (118)$$

The different Wick contractions of  $V_4$  give rise to

$$\Pi_4 = \frac{1}{\sqrt{\lambda}} \left( \frac{\mathcal{B}^2 I_4}{(1-\mathcal{B}^2)^3} + \frac{2\mathcal{B}^2 I_5}{(1-\mathcal{B}^2)^3} - \frac{2\mathcal{B}^2 I_3}{(1-\mathcal{B}^2)^3} + \frac{4\mathcal{B}^2 I_6}{(1-\mathcal{B}^2)^3} \right), \quad (119)$$

where

$$I_6 = \int d^2\sigma \log z (\partial_z K_N(t_1) \partial_t K_0(t_2) - \partial_z K_0(t_1) \partial_t K_N(t_2)) = \frac{1}{8\pi} (\log 16 L_{12} - L_{12}^2). \quad (120)$$

In (119), the terms proportional to  $I_4$ ,  $I_5$ ,  $I_3$  and  $I_6$  come from  $n^C \epsilon^{CDE} \langle \overbrace{y^A(t_1) y^B(t_2) (y^F y^F \partial_z y^D \partial_t y^E)} \rangle$ ,  $n^C \epsilon^{CDE} \langle \overbrace{(y^F y^F \partial_z y^D \partial_t y^E) y^A(t_1) y^B(t_2)} \rangle$ ,  $n^C \epsilon^{CDE} \langle \overbrace{y^A(t_1) y^B(t_2) (y^F y^F \partial_z y^D \partial_t y^E)} \rangle$  and

$n^C \epsilon^{CDE} \langle (\overline{y^F} y^F \partial_z y^D \overline{\partial_t y^E}) y^A(t_1) y^B(t_2) \rangle$  respectively. Evaluating (119) we get

$$\Pi_4 = \frac{\mathcal{B}^2}{\sqrt{\lambda}} \frac{1}{4\pi} \frac{1}{(1 - \mathcal{B}^2)^3} ((1 + \mathcal{B}^2) + 2 - (1 + \mathcal{B}^2) - 2) L_{12}^2 + \dots = 0 + \dots, \quad (121)$$

Thus, the total contribution to the term proportional to  $(\delta^{AB} - n^A n^B) L_{12}^2$  is

$$\Pi = \frac{1}{4\pi(1 - \mathcal{B}^2)^2} L_{12}^2 + \dots. \quad (122)$$

Therefore, the expected value of the coefficient  $f_2$  (62) seems to originate from self-energy diagrams exclusively. The same was observed in the case of Neumann boundary conditions [17].

## References

- [1] J. M. Maldacena, “*The Large N limit of superconformal field theories and supergravity*”, Adv. Theor. Math. Phys. **2** (1998) 231, [[hep-th/9711200](#)].
- [2] S. S. Gubser, I. R. Klebanov and A. M. Polyakov, “*Gauge theory correlators from noncritical string theory*”, Phys. Lett. B **428** (1998) 105, [[hep-th/9802109](#)].
- [3] E. Witten, “*Anti-de Sitter space and holography*”, Adv. Theor. Math. Phys. **2** (1998) 253, [[hep-th/9802150](#)].
- [4] I. R. Klebanov and E. Witten, “*AdS / CFT correspondence and symmetry breaking*”, Nucl. Phys. B **556** (1999) 89, [[hep-th/9905104](#)].
- [5] E. Witten, “*Multitrace operators, boundary conditions, and AdS/CFT correspondence*”, [hep-th/0112258](#).
- [6] S. S. Gubser and I. Mitra, “*Double trace operators and one loop vacuum energy in AdS/CFT*”, Phys. Rev. D **67**, 064018 (2003), [[hep-th/0210093](#)].
- [7] S. S. Gubser and I. R. Klebanov, “*A Universal result on central charges in the presence of double trace deformations*”, Nucl. Phys. B **656**, 23 (2003), [[hep-th/0212138](#)].
- [8] T. Hartman and L. Rastelli, “*Double-trace deformations, mixed boundary conditions and functional determinants in AdS/CFT*”, JHEP **0801**, 019 (2008), [[hep-th/0602106](#)].
- [9] D. H. Correa, V. I. Giraldo-Rivera and G. A. Silva, “*Supersymmetric mixed boundary conditions in AdS<sub>2</sub> and DCFT<sub>1</sub> marginal deformations*”, JHEP **03** (2020), 010, [[arXiv:1910.04225](#) [[hep-th](#)]].
- [10] O. Aharony, O. Bergman, D. L. Jafferis and J. Maldacena, “*N=6 superconformal Chern-Simons-matter theories, M2-branes and their gravity duals*”, JHEP **10** (2008), 091, [[arXiv:0806.1218](#) [[hep-th](#)]].
- [11] O. Aharony, O. Bergman and D. L. Jafferis, “*Fractional M2-branes*” JHEP **11** (2008), 043, [[arXiv:0807.4924](#) [[hep-th](#)]].
- [12] N. Drukker, J. Plefka and D. Young, “*Wilson loops in 3-dimensional N=6 supersymmetric Chern-Simons Theory and their string theory duals*”, JHEP **11** (2008), 019, [[arXiv:0809.2787](#) [[hep-th](#)]].

- [13] B. Chen and J. B. Wu, “*Supersymmetric Wilson Loops in  $N=6$  Super Chern-Simons-matter theory*”, Nucl. Phys. B **825** (2010), 38-51, [[arXiv:0809.2863 \[hep-th\]](#)].
- [14] S. J. Rey, T. Suyama and S. Yamaguchi, “*Wilson Loops in Superconformal Chern-Simons Theory and Fundamental Strings in Anti-de Sitter Supergravity Dual*”, JHEP **03** (2009), 127, [[arXiv:0809.3786 \[hep-th\]](#)].
- [15] N. Drukker and S. Kawamoto, “*Small deformations of supersymmetric Wilson loops and open spin-chains*”, JHEP **07** (2006), 024, [[hep-th/0604124](#)].
- [16] S. Giombi, R. Roiban and A. A. Tseytlin, “*Half-BPS Wilson loop and  $AdS_2/CFT_1$* ” Nucl. Phys. B **922** (2017), 499-527, [[arXiv:1706.00756 \[hep-th\]](#)].
- [17] M. Beccaria, S. Giombi and A. A. Tseytlin, “*Correlators on non-supersymmetric Wilson line in  $\mathcal{N} = 4$  SYM and  $AdS_2/CFT_1$* ”, JHEP **05** (2019), 122, [[arXiv:1903.04365 \[hep-th\]](#)].
- [18] L. Bianchi, G. Bliard, V. Forini, L. Griguolo and D. Seminara, “*Analytic bootstrap and Witten diagrams for the ABJM Wilson line as defect  $CFT_1$* ”, JHEP **08** (2020), 143, [[arXiv:2004.07849 \[hep-th\]](#)].
- [19] N. Drukker and D. Trancanelli, “*A Supermatrix model for  $N=6$  super Chern-Simons-matter theory*”, JHEP **02** (2010), 058, [[arXiv:0912.3006 \[hep-th\]](#)].
- [20] H. Ouyang, J. B. Wu and J. j. Zhang, “*Novel BPS Wilson loops in three-dimensional quiver Chern-Simons-matter theories*”, Phys. Lett. B **753** (2016), 215-220, [[arXiv:1510.05475 \[hep-th\]](#)].
- [21] H. Ouyang, J. B. Wu and J. j. Zhang, “*Construction and classification of novel BPS Wilson loops in quiver Chern-Simons-matter theories*”, Nucl. Phys. B **910** (2016), 496-527, [[arXiv:1511.02967 \[hep-th\]](#)].
- [22] L. Castiglioni, S. Penati, M. Tenser and D. Trancanelli, “*Interpolating Wilson loops and enriched RG flows*” JHEP **08** (2023), 106, [[arXiv:2211.16501 \[hep-th\]](#)].
- [23] L. Castiglioni, S. Penati, M. Tenser and D. Trancanelli, “*Wilson loops and defect RG flows in ABJM*”, JHEP **06** (2023), 157, [[arXiv:2305.01647 \[hep-th\]](#)].
- [24] N. Drukker, D. Trancanelli, L. Bianchi, M. S. Bianchi, D. H. Correa, V. Forini, L. Griguolo, M. Leoni, F. Levkovich-Maslyuk and G. Nagaoka, *et al.* “*Roadmap on Wilson loops in 3d Chern-Simons-matter theories*”, J. Phys. A **53** (2020) no.17, 173001, [[arXiv:1910.00588 \[hep-th\]](#)].
- [25] C. S. Chu and P. M. Ho, “*Noncommutative open string and D-brane*”, Nucl. Phys. B **550** (1999), 151-168, [[hep-th/9812219](#)].
- [26] V. Schomerus, “*D-branes and deformation quantization*”, JHEP **06** (1999), 030, [[hep-th/9903205](#)].
- [27] N. Seiberg and E. Witten, “*String theory and noncommutative geometry*” JHEP **09** (1999), 032, [[hep-th/9908142](#)].
- [28] A. Lewkowycz and J. Maldacena, “*Exact results for the entanglement entropy and the energy radiated by a quark*” JHEP **05** (2014), 025, [[arXiv:1312.5682 \[hep-th\]](#)].

- [29] A. Cavaglià, N. Gromov, J. Julius and M. Preti, “*Integrability and conformal bootstrap: One dimensional defect conformal field theory*”, Phys. Rev. D **105** (2022) no.2, L021902 [[arXiv:2107.08510\[hep-th\]](#)].
- [30] A. Cavaglià, N. Gromov, J. Julius and M. Preti, “*Bootstrability in defect CFT: integrated correlators and sharper bounds*”, JHEP **05** (2022), 164, [[arXiv:2203.09556\[hep-th\]](#)].
- [31] A. Cavaglià, N. Gromov, J. Julius and M. Preti, “*Integrated correlators from integrability: Maldacena-Wilson line in  $\mathcal{N} = 4$  SYM*”, JHEP **04** (2023), 026, [[arXiv:2211.03203\[hep-th\]](#)].
- [32] V. Niarchos, C. Papageorgakis, P. Richmond, A. G. Stapleton and M. Woolley, “*Bootstrability in line-defect CFTs with improved truncation methods*”, Phys. Rev. D **108** (2023) no.10, 105027, [[arXiv:2306.15730\[hep-th\]](#)].
- [33] A. Cavaglià, N. Gromov and M. Preti, “*Computing Four-Point Functions with Integrability, Bootstrap and Parity Symmetry*”, [[arXiv:2312.11604\[hep-th\]](#)].
- [34] D. H. Correa, V. I. Giraldo-Rivera and M. Lagares, “*Integrable Wilson loops in ABJM: a Y-system computation of the cusp anomalous dimension*”, JHEP **06** (2023), 179, [[arXiv:2304.01924\[hep-th\]](#)].
- [35] J. A. Minahan, O. Ohlsson Sax and C. Sieg, “*A limit on the ABJ model*”, J. Phys. Conf. Ser. **462** (2013) no.1, 012035, [[arXiv:1005.1786\[hep-th\]](#)].
- [36] A. F. Canazas Garay, D. H. Correa, A. Faraggi and G. A. Silva, “*Interpolating boundary conditions on  $AdS_2$* ”, JHEP **02** (2023), 146, [[arXiv:2210.12043\[hep-th\]](#)].
- [37] S. Randjbar-Daemi, A. Salam and J. A. Strathdee, “ *$\sigma$  Models and String Theories*”, Int. J. Mod. Phys. A **2** (1987), 667.
- [38] A. A. Tseytlin, “*Renormalization of String Loop Corrections on the Disk and the Annulus*”, Phys. Lett. B **208** (1988), 228-238.